Crack growth resistance and dynamic rupture arrest under slip dependent friction

C. Voisin [a,*], I. Ionescu [b], M. Campillo [a]

[a] *Laboratoire de Géophysique Interne, Observatoire de Grenoble, Université Joseph Fourier, BP 53X, 38041 Grenoble Cedex, France*
[b] *Laboratoire de Mathématiques Appliquées, Université de Savoie, Chambéry, France*

Abstract

The slip-strengthening behavior observed in fracture and friction experiments is considered as a possible candidate for crack growth resistance and dynamic rupture arrest. The peak shear stress τ_p and the strengthening slip D_s play a role in the crack growth resistance. Depending on this resistance, the rupture may be stopped by a strengthening barrier. In such a case, we show that the residual shear stress at the end of the dynamic process is not grid-size dependent, suggesting that the static shear stress will not exhibit any singularity at the crack tip. Hence, rupture arrest by a strengthening barrier is compatible with a criterion based on finite shear stress threshold. Considering a finite weak zone bounded by two strengthening barriers, we investigate the modalities of the rupture arrest. Despite the presence of the barriers, the size of the rupture event is not controlled a priori but rather depends on both the strength of the barrier and the seismic energy released in the weak zone. Depending on the parameters of the strengthening, two mechanisms are possible for the rupture arrest. The first one is associated with a negative stress drop inside the resisting zone. This mechanism is independent from the size of the weak zone. The second mechanism is associated with a positive stress drop inside the resisting zone, and is crack-size dependent. In both cases, we show the existence of a crack-arrest zone characterized by small amount of slip and shear stress concentration and associated with a self-healing slip pulse. This model, with weak zones and resisting zones is consistent with recent strong motion inversions and offers a possible mechanism for the fault length increase over geological times through progressive barrier damaging.
© 2002 Elsevier Science B.V. All rights reserved.

Keywords: Crack growth resistance; Slip dependent friction; Dynamic rupture

1. Introduction

The rupture arrest problem has been intensively studied through the last decades. Three wide classes of studies can be distinguished. The first class considers the effects of the fault geometry on the rupture propagation. It has been shown that the rupture propagation could be stopped by an angle in the fault plane (Streiff and Bouchon, 1997). More recently, Kame and Yamashita (1999) have used an integral method to study the spontaneous rupture arrest. They show that over a certain length the rupture quits the main propagation axis: the faulting surface is no more planar. In this model, the length of rupture is not fixed a priori and the rupture propagation stops because the surface is misoriented with regards to the ambient stress field. However, this is valid only when the ambient stress field is largely greater than the stress field emitted by the rupture propagation. Bouchon et al. (1998) have studied the Landers rupture process in

* Corresponding author. Tel.: +33-476-82-8036;
fax: +33-476-82-8101.
E-mail address: christophe.voisin@ujf-grenoble.fr (C. Voisin).

details. They have shown that the third segment was triggered by the intense dynamic stress field emitted by the Emerson-Camp Rock segment, and that it ruptured in spite of a misorientation of the segment with regards to the regional stress field.

The stress acting on the fault surface constitutes the second axis of study of rupture arrest. The difference between the initial state of stress τ_i and the static stress τ_s appears a key control parameter in the rupture propagation (e.g. Burridge, 1973; Day, 1982), and more recently (Olsen et al., 1997). Perrin et al. (1995) used understressed termination zones to stop the rupture propagation. The question of shear stress singularity has been addressed by Bonafede et al. (1985) and Chen and Knopoff (1986). Indeed, since the friction law deals with finite shear stress values a singularity is not consistent with a frictional model of the fault. Chen and Knopoff (1986) have considered an understressed fault with slip-weakening friction and performed a static analysis. They showed that for a given prestress (defined as the difference between τ_i and τ_s) it exists only one critical patch length for the crack associated with finite values of the shear stress at the tips in the static configuration. Any other crack length is associated with stress singularities, in spite of the slip-weakening friction.

Lateral variation of friction properties along the fault surface have been investigated. For instance, unbreakable rigid barriers are likely to stop the rupture propagation (e.g. Husseini et al., 1975; Das and Aki, 1977). Two problems arise from the use of rigid barriers: (1) the size of rupture event is controlled a priori by the position of the barriers on the fault; (2) the residual stress field is necessarily singular at the crack tips, even if we use a cohesive or a breakdown zone model (e.g. Barenblatt, 1959; Ida, 1972).

The aim of this paper is to give a numerical study of the dynamic rupture arrest for the two-dimensional antiplane case. Our intention is to propose some models, laid on a physical basis, which remove the shear stress singularities and may be used in numerical computations of more realistic three-dimensional geometries where the analytical methods are not efficient. Basically, we intend to use the strengthening behavior that is observed both in shear fracture experiments (Ohnaka et al., 1997) and in shear frictional experiments (Ohnaka and Yamashita, 1989). Ohnaka et al. (1997) have performed series of shear fracture of intact rock samples, under lithospheric pressure and temperature conditions. The shear stress is found to first increase with the displacement until a peak shear stress τ_p is reached at a displacement D_s. Then the shear stress progressively degrades with the ongoing slip until it reaches the residual shear stress τ_d at a slip displacement D_c, known as the critical slip. At this moment, the rock sample is broken and a new frictional surface is created that runs through the whole sample. It is worth noting that the static stress drop $\Delta\tau = \tau_i - \tau_d$ (the difference between the initial shear stress and the residual shear stress) is negative. This is somewhat not surprising: to create a new frictional surface in a fresh rock sample needs more energy than the friction on this newly created surface may release. The same generic behavior is observed in friction experiments. Ohnaka and Yamashita (1989) presents the results of high precision experiments and emphasizes the beginning of the constitutive friction relation between the shear stress τ and the displacement. Outside of the nucleation zone, the friction first increases with the displacement up to a peak value τ_p, before to degrade with the ongoing slip. However, in friction experiments the stress drop $\Delta\tau$ is always positive. Obviously, if the constitutive relation is the same for fracture and friction, the orders of magnitude of the involved parameters (D_s, D_c, τ_p) are quite different. Nonetheless, a slip dependent constitutive relation holds for both frictional and fracture processes. As a point of fact, it has been shown that shear frictional resistance conforms to shear fracture resistance under lithospheric conditions (Ohnaka, 1992). In other words, the shear fracture process is the upper limit to shear frictional process, and both of them can be interpreted in the slip dependence framework.

We study here how the slip-strengthening controls the local resistance to crack growth. Moreover we aim to test the ability of a strengthening barrier to stop the rupture propagation. In the following, the fault surface will be composed of a weak zone characterized by a pure slip-weakening friction law that allows the rupture to nucleate and propagate. This weak zone is limited by resisting zones associated with a strengthening behavior prior to the slip-weakening behavior. However, despite the presence of these resisting zones, the final size of rupture is not prescribed a priori, but rather depends on the strengthening parameters of the barriers and on the seismic energy released in the weak

zone. For the sake of simplicity, we will consider that the initial state of stress τ_i along the fault is homogeneous and equals the static stress friction τ_s. At time $t = 0$ s, a small slip perturbation is applied at the center of the weak zone of the fault. This perturbation gives birth to a slip instability that grows exponentially with time as the slip-weakening friction law is going on. We do not discuss here details on the growth of instability and transition from initiation to propagation (see Campillo and Ionescu, 1997; Knopoff et al., 2000; Ampuero et al., 2001 for the infinite case, and Ionescu and Campillo, 1999; Dascalu et al., 2000; Voisin et al., 2002 for the finite case). We aim here to discuss the ability of the strengthening zones to stop the rupture propagation. We show numerically that depending on the strengthening parameters (namely the slip of strengthening D_s and the slope of strengthening S_s) two mechanisms are possible for the rupture to be stopped. The first one is already well-known and is associated with a negative or null stress drop in the resisting zone. This mechanism is crack-size independent. The second mechanism is associated with positive stress drop in the resisting zone and is crack-size dependent. In both cases, the rupture is stopped over a crack-arrest zone that is associated with a self-healing slip pulse, which amplitude and duration are functions of the strengthening parameters. The slip distribution is not limited to the weak zone of the fault but rather spreads inside the resisting zones. This property seems to remove the shear stress singularities associated with classical models of cracks and fractures. This allows also the fault growth through progressive damaging of the strengthening barriers.

2. Mathematical model

Consider the antiplane shearing on a fault surface Γ_f a homogeneous linear elastic space. The Γ_f lies in the plane $y = 0$. The contact with friction on the fault is described by an heterogeneous slip dependent friction law. We assume that the displacement field is 0 in directions O_x and O_y and that u_z does not depend on z. The displacement is therefore denoted simply by $w(t, x, y)$. The elastic media has the shear rigidity G, the density ρ, and the shear velocity $c = \sqrt{G/\rho}$. The nonvanishing shear stress components are $\tau_{zx} = \tau_x^\infty + G\partial_x w(t, x, y)$ and $\tau_{zy} = \tau_y^\infty + G\partial_y w(t, x, y)$,

where τ_x^∞, τ_y^∞ are the components of the initial stress field. Keeping in mind that we deal with the evolution of an initial pulse, we impose (for symmetry reasons) $w(t, x, y) = -w(t, x, -y)$ and restrict ourselves to the upper half-space $y > 0$. We also assume that the slip $w(t, x, 0)$ and the slip rate $\partial_t w(t, x, 0)$ are nonnegative. Since we suppose the initial stress to be in equilibrium the equation of motion in the elastic half space is

$$\frac{\partial^2 w}{\partial t^2}(t, x, y) = c^2 \nabla^2 w(t, x, y) \tag{1}$$

for $t > 0$ and $y > 0$. The friction boundary conditions on the fault Γ_f can be written as

$$G\partial_y w(t, x, 0) = f(x, \delta) - \tau_y^\infty, \quad \text{if } \partial_t w(t, x, 0) > 0 \tag{2}$$

$$G\partial_y w(t, x, 0) \leq f(x, \delta) - \tau_y^\infty, \quad \text{if } \partial_t w(t, x, 0) = 0 \tag{3}$$

where $f(x, \delta)$ is the slip dependent friction law on the heterogeneous fault. The initial conditions are prescribed by

$$\frac{\partial w}{\partial t}(0, x, y) = w_1(x, y) \tag{4}$$

where w_1 is a given function of (x, y). We shall consider in the following w_1 as a small perturbation of the equilibrium position $w \equiv 0$.

Let us remark that only the distribution of the stress excess $f(x, \delta) - \tau_y^\infty$ is implied in the boundary conditions on the fault. Hence one can imagine either a homogeneous initial stress and a nonhomogenous friction $f(x, \delta)$ or a nonhomogenous initial stress $\tau_y^\infty(x, y)$ and an homogenous friction $f(\delta)$, with the condition that the stress excess remains the same in both descriptions. All over this paper we have considered the first case but all results are valid in the second case either. We consider a homogenous initial stress field $\tau_i = \tau_y^\infty$ and a nonhomogenous friction law $f(x, \delta) = \mu(x, \delta)S$ where S is the normal stress on the fault plane (i.e. $\tau_{yy} = -S$ with $S > 0$) and $\mu(x, \delta)$ is the slip dependent friction coefficient. Hence, the stress excess becomes

$$\mu(x, \delta)S - \tau_i, \quad \forall x \in \Gamma_f, \delta \geq 0 \tag{5}$$

We use here a slip dependent friction law derived from the experimental works by (Ohnaka, 1996),
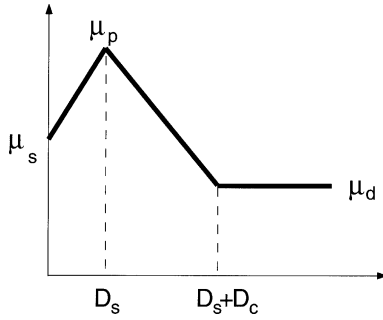
Fig. 1. The generic slip dependent friction law used in this study. D_s is the strengthening slip, D_c is the critical slip. The first part of the law is in strengthening from μ_i (initial friction coefficient) to μ_p (peak friction coefficient) and represents the local strength of the fault. The second part is in weakening from μ_p to μ_d (dynamic friction coefficient). A weak zone is defined by $\mu_s = \mu_p$: it has only the slip-weakening part of the law. A barrier is defined by $\mu_p > \mu_s$, and therefore by the slip-strengthening part of the law.

which has the form of a piecewise linear function, as presented in Fig. 1:

$$\mu(x, \delta) = \mu_s(x) + S_s(x)\delta, \quad \text{if} \quad 0 \le \delta \le D_s(x) \tag{6}$$

$$\mu(x, \delta) = \mu_p(x) - S_w(x)\delta,$$
$$\text{if } D_s(x) < \delta \le D_s(x) + D_c(x) \tag{7}$$

$$\mu(x, \delta) = \mu_d(x), \quad \text{if} \quad D_s(x) + D_c(x) \le \delta \tag{8}$$

where $\mu_s(x)$, $\mu_p(x)$ and $\mu_d(x)$ are the static, the peak and dynamic friction coefficients at position x, $S_s(x)$, $S_w(x)$ are the strengthening and the weakening slopes and $D_s(x)$, $D_c(x)$ are the strengthening slip and the critical slip. We have

$$\mu_p(x) = \mu_s(x) + S_s(x)D_s(x),$$
$$\mu_d(x) = \mu_p(x) - S_w(x)D_c(x) \tag{9}$$

The fault Γ_f is divided in three parts (Fig. 2): a weak zone $\Gamma_w = \{|x| < a, y = 0\}$ of length $2a$ bounded by two resisting zones $\Gamma_r = \{|x| \ge a, y = 0\}$ characterized by their strengthening slip $D_s(x)$ as follows:

$$D_s(x) = 0, \quad \text{if} \quad x| < a$$
$$D_s(x) > 0, \quad \text{if} \quad x| \ge a \tag{10}$$

In all our simulations (except in Section 3.1) $\mu_s(x)$ and $D_c(x)$ are kept as constants, i.e.

$$\mu_s(x) = \mu_s, \quad D_c(x) = D_c \tag{11}$$

We introduce here the dimensionless stress drop parameter η as

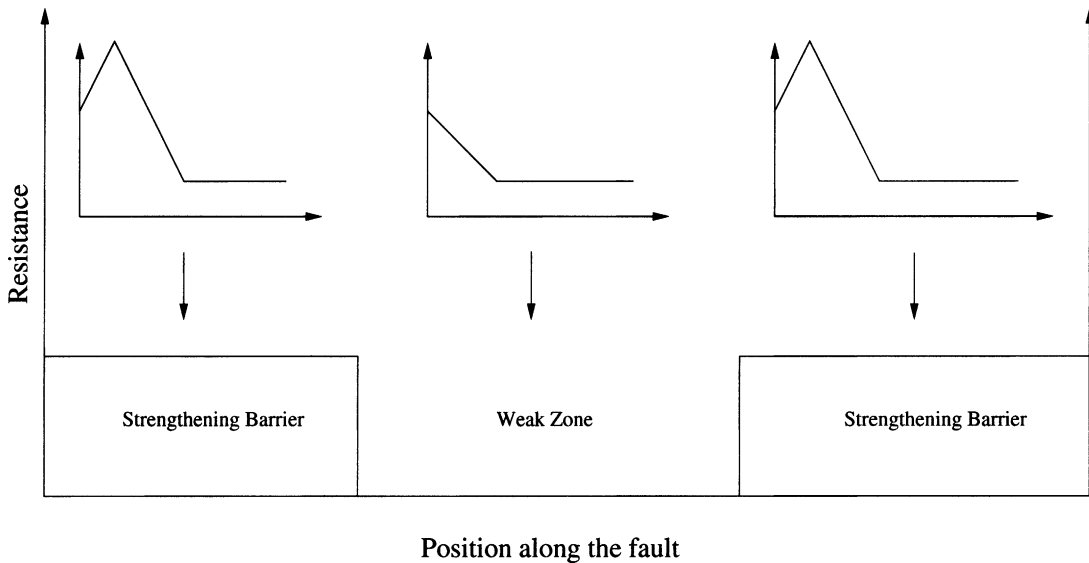$$\eta(x) = \frac{\tau_i - S\mu_d(x)}{S\mu_p(x) - S\mu_d(x)} \tag{12}$$

Fig. 2. Distribution of the strengthening slip and of the corresponding friction laws along the fault surface. A weak zone characterized by only slip weakening is limited by two strengthening barriers characterized by both slip strengthening and slip weakening.

Since our intention is to study the evolution of the elastic system near an unstable equilibrium position, we shall suppose that $\tau_i = S\mu_s$. Therefore, η can be defined as

$$\eta(x) = \frac{\mu_s(x) - \mu_d(x)}{\mu_p(x) - \mu_d(x)} \quad (13)$$

By definition, $\eta = 1$ in the weak part of the fault (where $\mu_p = \mu_s$); $0 < \eta < 1$ in the resisting zones associated with a positive stress drop (i.e. when $\mu_s > \mu_d$); $\eta < 0$ in the resisting zones associated with a negative stress drop (i.e. $\mu_s < \mu_d$).

We remark that $w \equiv 0$ is an equilibrium position, and w_1 may be considered as small perturbation of the equilibrium. In order to deal with an unstable equilibrium state we shall suppose that $a\alpha > \beta_0 \approx 1.15777$ in the weak zone (see Dascalu et al., 2000 for more details) where

$$\alpha = \frac{S(\mu_s - \mu_d)}{GD_c} \quad (14)$$

This simply signifies that either the weak zone length $2a$ or the weakening rate of the friction are large enough to promote the growth of a slip instability. By this way we insure the existence of a propagating crack in the weak zone.

3. The residual shear stress concentration and its grid-dependence

The numerical results presented here have been computed with the finite difference scheme proposed by Ionescu and Campillo (1999) to solve the nonlinear problem (1)–(4). We use a grid of 800×800 points in the x, y plane and the following model parameters: $\rho = 3000\,\text{kg/m}^3$, $C = 3000\,\text{m/s}$, $\mu_s - \mu_d = 0.04$. The half length of the fault is $a = 1000\,\text{m}$. The normal stress is computed at a depth of 5000 m, which gives $S_N \approx 150\,\text{MPa}$. The initial condition corresponds to a velocity perturbation w_1 with the following distribution

$$w_1(x, y) = \begin{cases} A \exp \dfrac{x^2}{x^2 - h^2} \exp\left(\dfrac{-y}{h}\right); \\ \quad |x| < h,\ |y| < h, \\ 0, \quad \text{elsewhere} \end{cases} \quad (15)$$

where the half width h is 100 m and the maximum amplitude A is 0.001 m/s. The numerical scheme

allows for the time evolution computation of shear stress and slip velocity along the fault plane.

3.1. The case of a rigid barrier

We consider in this section the classical case of a rigid barrier. We put $\mu_s(x)$ very large ($\mu_s(x) \to \infty$) outside of the weak zone of the fault, i.e.

$$\begin{aligned} |x| < a; & \quad \mu_s(x) = \mu_s \\ |x| \geq a; & \quad \mu_s(x) = \infty \Leftrightarrow w = 0,\ \forall t \in [0; +\infty[\end{aligned}$$

$$(16)$$

where a is the half fault length. In other words, the weak zone of the fault is limited by two unbreakable barriers. This case has already been intensively studied (e.g. Madariaga, 1976). We performed four simulations of rupture propagation on the weak zone of the fault with different space steps: $\Delta x = 2, 10, 50$ and 100 m. As expected, we remarked an important dependence of the stress peak on the grid. Indeed the smaller the step is, the larger the stress peak is (see Table 1, first line). As a point of fact, when the rupture stops the shear stress exhibits a singularity in the vicinity of the crack tip zone, even if we use a slip dependent friction law as we did. Ida (1972) and Rice and Simmons (1976) used the breakdown zone model and showed the absence of crack tip shear stress singularity associated with the propagation of the rupture front. The shear stress singularity that we discuss here is the one that arises as the rupture abruptly stops at the rigid, unbreakable barrier. As a consequence, we cannot define a stress criterion involving a stress threshold to describe the final equilibrium state. In crack theory the threshold in stress is replaced by a threshold in stress intensity factor. However, earthquakes are far more

Table 1
Maximum of the shear stress concentration (in MPa) as a function of the space step

Δx (m)	2	10	50	100
Rigid barrier	130	35.5	19.6	14.6
Sharp strengthening barrier	60	16.3	9.8	7.3
Smooth strengthening barrier	12.2	11.8	11.0	10.0

First line: the rigid barrier case. A strong grid-size dependence is noted. Second line: sharp strengthening barrier. A weaker grid-size dependence is noted. Third line: smooth strengthening barrier. The grid-size dependence is not present.

complex than a simple crack and can be understood as complex slipping processes with variable resistance on the barriers (Beroza and Mikumo, 1996). At any given time during the rupture, some parts of the fault may be slipping while others may be still resisting. The complex path of rupture propagation, especially in three-dimensional, impeaches us to foreknow the status of the different patches of the fault surface. Consequently, we cannot use both concepts of stress and stress intensity for the frictional slipping patches and for the resistant nonslipping patches, respectively, because this would need the foreknowledge of each fault patch status at every time.

3.2. The case of a sharp transition to the strengthening barrier

We consider the case of a weak zone (of length $2a$) limited by two strengthening barriers. The barriers are characterized by a constant slope of strengthening $S_s(x) = S_s$ and a constant strengthening slip $D_s(x) = D_s > 0$. In the weak zone, there is no slip strengthening. Hence, we have

$$|x| < a; \qquad \mu_p(x) = \mu_s$$
$$|x| \leq a; \quad \mu_p(x) = \mu_s + S_s D_s \qquad (17)$$

Such a distribution of the peak of friction $\mu_p(x)$ describes sharp transitions from the slip weakening zone to the barriers, located at $x = \pm a$. As in Section 3.1, we have performed four simulations of the dynamic rupture process on the same weak zone of length $2a = 2000$ m, with the same space steps: $\Delta x = 2, 10, 50$ and 100 m. For each simulation the maximum of the shear stress concentration was reported in Table 1, second line. For a given space step, the maximum of the shear stress is always lower if we use a strengthening barrier than if we use a rigid barrier. However, we note that the maximum of shear stress is again dependent on the space step. This can be related to the sharp transition from the weak zone to the barrier. This sudden discontinuity in the frictional behavior (from slip weakening to slip strengthening as the rupture quits the weak zone and enters the resisting zone) introduces a space discontinuity in the coefficients of the boundary condition (2). The slip is supposed to be continuous, and we get a space discontinuity in the spatial derivative of the slip distribution with respect to x. Since in the static case or equivalently at the end

of the dynamic process, the shear stress is given by the Hilbert transform of the spatial derivative of the slip distribution, a discontinuity in this distribution introduces a low-order singularity in the shear stress. This could explain why the shear stress is less dramatically dependent on the space step than in the rigid case. To confirm this point, we have performed in the Section 3.3 a simulation with a smooth transition from the weak zone to the barrier.

3.3. The case of a smooth transition to the strengthening barrier

The weak zone has a length $2a = 2000$ m and is bounded by two smooth strengthening barriers. By smooth, we intend that the transition is described by more than one grid point, in such a way that the transition appears continuous even with the coarse grid step $\Delta x = 100$ m. We have performed four simulations with the same space steps: $\Delta x = 2, 10, 50$ and 100 m, respectively.

As in the two previous cases, a shear stress concentration at the tips of the rupture patch linked to the rupture arrest is observed (Fig. 3). The maximum of the shear stress concentration is given in Table 1, third line. It is quite the same for all simulations, even with a space step of 2 m, that is 50 times smaller than the coarse space step of 100 m. In this latter case, the shear stress profile is poorly described. As discussed by Madariaga et al. (1998), the oscillations in the stress profile are due to intrinsic discreteness that appears when the grid step is too large. However, the rupture arrest is a slightly different problem than the rupture propagation. Fig. 3 shows that the stress profile is well described even with the coarse step of 100 m. The discrepancy in the approximation of the maximum of the stress concentration with different grid steps is probably due to the poor description of the weakening process in the weak zone with larger grid steps.

Despite possible numerical artifacts, the results in Table 1, third line, may indicate that the shear stress singularity has been removed and that no grid-dependence is present. Though analytical investigation is required to prove that the singularities are removed, these encouraging numerical results provide a model of rupture arrest consistent with a friction law. Fig. 4 shows both the slip and the shear stress after a dynamic rupture process, and emphasizes the
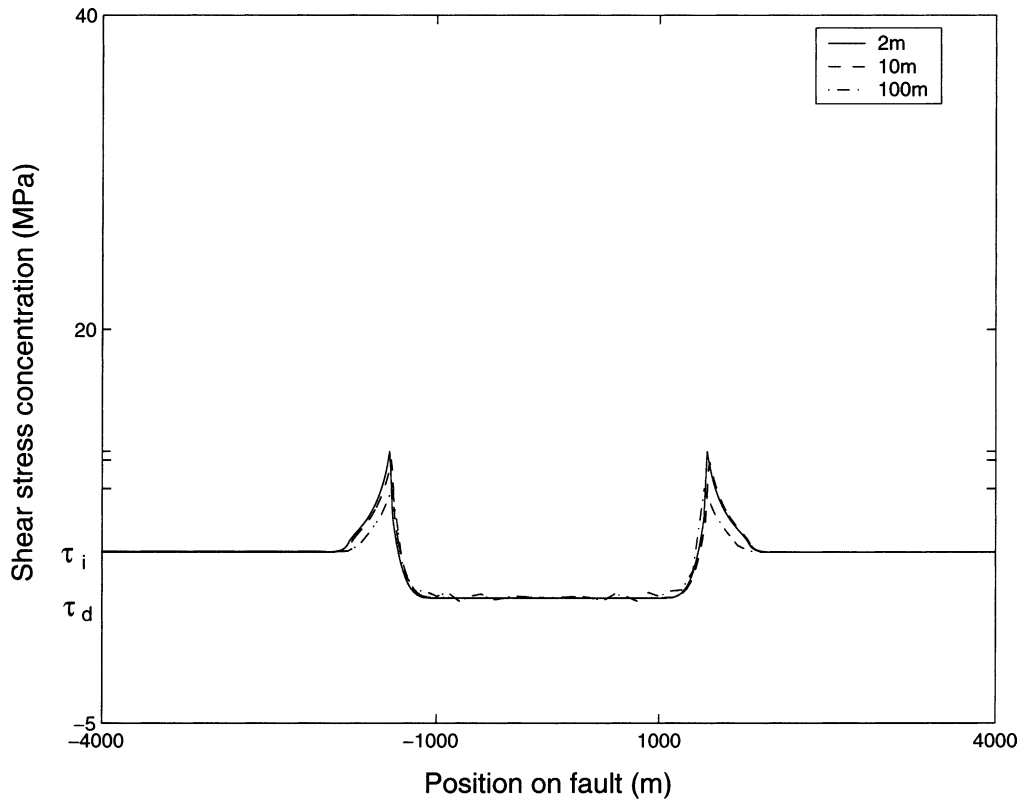
Fig. 3. Distribution of the shear stress after a dynamic rupture process on a weak fault of length $2a = 2000$ m bounded by two smooth strengthening barriers. The different curves correspond to different space steps ($\Delta x = 2$, 10 and 100 m). We note a shear stress concentration at the tips of the ruptured patch. This shear stress peak is poorly dependent on the space step. The coarse grid step of 100 m introduces intrinsic discreteness, as testified by the oscillations of the stress profile in the weak zone. However, even in this case the stress profile in the arrest zone is correctly described.

relation between the crack-arrest zone and the shear stress concentration. The crack-arrest zone is defined as the zone of gentle decrease in slip down to zero. It is associated with a shear stress concentration that obviously differs from a singularity and that decreases down to the initial state of stress. The main difference between rigid and strengthening barriers is the existence of this crack-arrest zone associated with the strengthening barriers. In the rigid case, the rupture stops at the barrier, whereas in the strengthening case, the rupture propagates inside the barrier over the crack-arrest zone. In other words, the crack-arrest zone corresponds to a zone of damaging of the barrier. The spatial extent of the crack-arrest zone is related to the strength of the barrier.

4. Rupture arrest in a strengthening barrier

We have shown that the model of slip-strengthening barrier offers numerical advantages since it avoids the stress dependence on the space grid interval. In the following, we test the ability of strengthening barriers to stop the rupture propagation through a parametric investigation.

4.1. Crack growth resistance

The strength of the barrier is defined through two parameters: D_s the strengthening slip and S_s the slope of the strengthening. To illustrate the effects of these two parameters, we performed simulations in
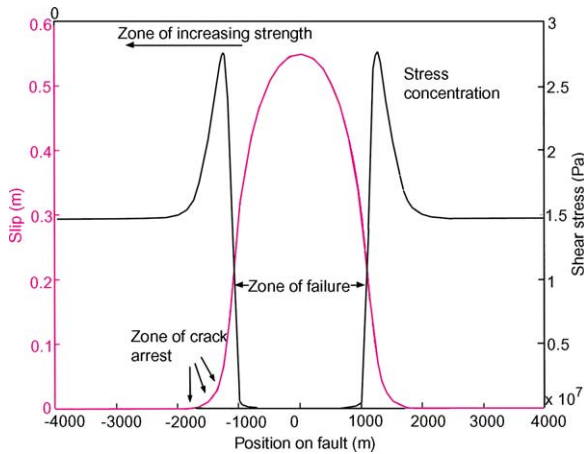
Fig. 4. Distribution of slip and of shear stress after a dynamic rupture process on a weak fault of length $2a = 2000$ m bounded by two strengthening barriers of increasing resistance. We note the crack-arrest zone (black arrows) associated with the shear stress concentration that differs from a singularity.

Fig. 5. The effect of the slope of strengthening on the arrest of the rupture propagation: (top) for a weak slope of strengthening ($S_s = 1$ m^{-1}) the rupture propagates through the harriers; (bottom) for a larger slope of strengthening ($S_s = 20$ m^{-1}) the rupture is stopped by the barriers. The computations were achieved for a grid step $\Delta x = 10$ m.

the case of a weak zone of length $2a = 3000$ m, characterized by a critical slip $D_c = 0.04$ m and a positive stress drop $\Delta\tau \approx 6$ MPa. The strengthening barriers have a strengthening slip $D_s = 0.01$ m and different values of S_s, the strengthening slope. Fig. 5 shows examples of behavior of the rupture with two different strengthening barriers. At time $t = 0$ s, a small perturbation is applied at the center of the fault. This perturbation evolves into a dynamic instability that grows exponentially with time as the friction decreases from τ_s down to τ_d. This phase is called the initiation phase and is described in Campillo and Ionescu (1997) for an infinite fault, and in Ionescu and Campillo (1999) for a finite fault. The transition to the propagation phase occurs when the stress has reached the dynamic friction at some patch on the weak zone. At this time a crack front appears and propagates away on the fault until it reaches the strengthening barriers. The first case of evolution of the slip rate along the fault is computed with a slope of strengthening $S_s = 1$ m^{-1}. In this case, the rupture propagates through the resisting zones. A larger slope strengthening ($S_s = 20$ m^{-1}) associated with a larger τ_p stops the rupture as it encounters the barriers. This shows the expected result that the strengthening barriers are able to stop a given rupture process, only if their resistance is large enough. Until now the crack
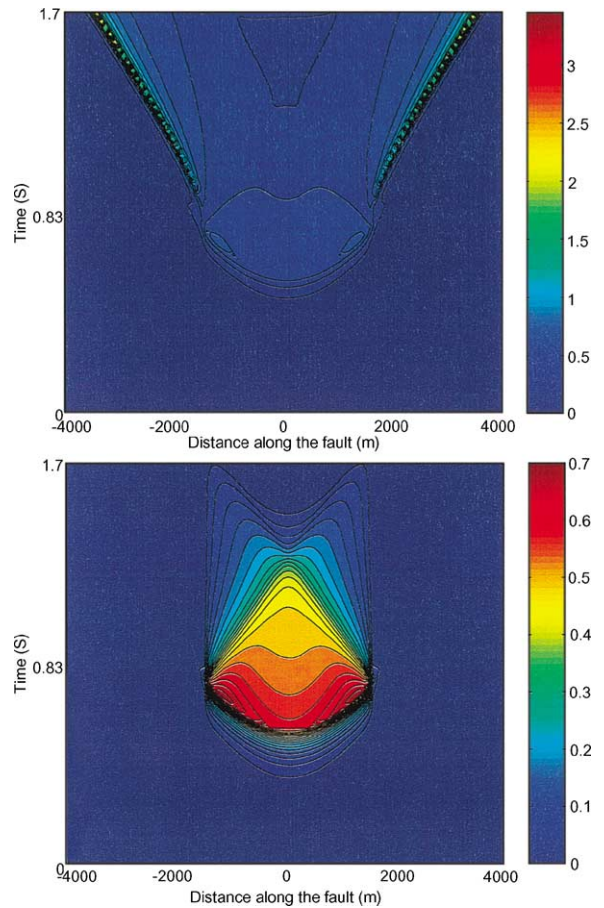
growth resistance was assumed to be the product of the strengthening slope S_s by the strengthening displacement D_s. In other words, the local crack growth resistance is represented by the local peak shear stress τ_p. In order to confirm or infirm this hypothesis, it is interesting to determinate the limits of efficiency of the barriers to stop a given rupture process. We consider a finite weak zone of length $2a = 3000$ m associated with a slip-weakening friction law characterized by a critical slip $D_c = 0.04$ m and a weakening slope $S_w = 1$ m^{-1}. This weak zone is limited by strengthening barriers which present the same static

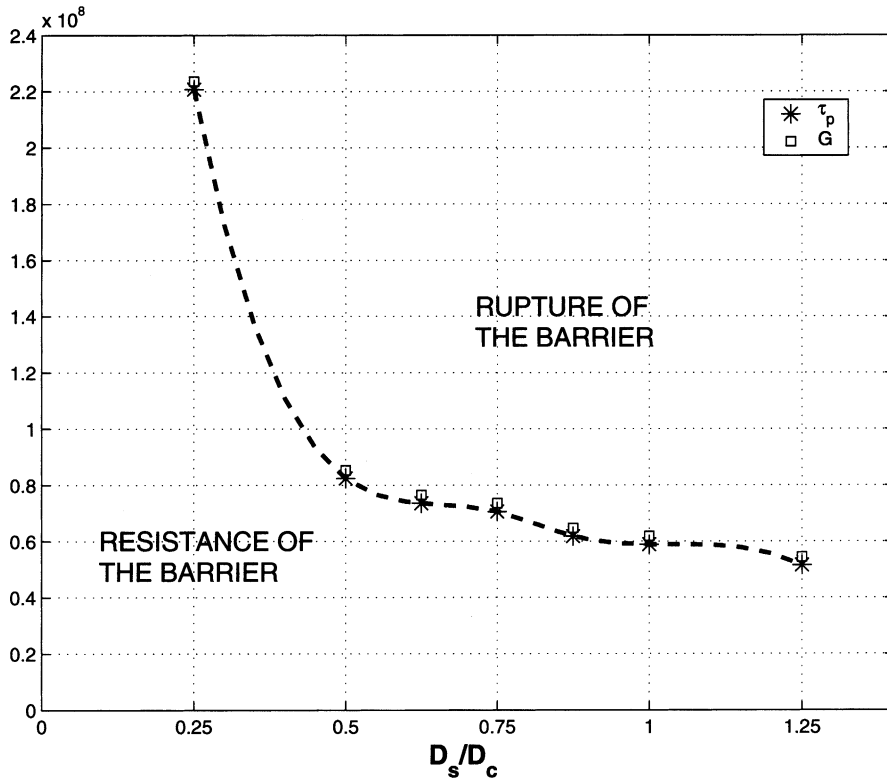Fig. 6. Test of resistance of a strengthening barrier. The initial weak zone size is $2a = 3000\,\text{m}$, and $D_c = 0.04\,\text{m}$. The main result is that neither τ_p nor G is constant as it could have been expected from the static analysis of (Chen and Knopoff, 1986). The variations of τ_p indicate that the resistance of the barrier is a function of both τ_p and D_s. The computations were achieved for a grid step $\Delta x = 10\,\text{m}$.

stress drop as the weak zone. The underlying idea is to determine the parameters D_s and S_s needed to stop the rupture propagation. The limit between the two behaviors (the rupture is stopped or the barrier are broken) is constructed as follows: we choose a value for the strengthening displacement D_s and we search the minimum value of the slope of strengthening S_s that can stop the rupture process. Fig. 6 presents the corresponding values of $\tau_p = \tau_s + S_s D_s$ and $G = (1/2)(S_s D_s + S_w D_c)$ (the fracture energy) as functions of D_s/D_c. It is obvious that the peak shear stress τ_p is not the only parameter responsible for the resistance of the strengthening barrier. When D_s is smaller than D_c as observed in the friction experiments the value of τ_p dramatically increases to stop the rupture process. The fracture energy G scales with τ_p, which implies that no simple energy criterion can be used to forecast the rupture behavior in the barrier. These results

mean that the crack growth resistance is not simply expressed by τ_p, but is rather a function of both the peak shear stress and the strengthening displacement. This is consistent with the rigid case: as the strengthening displacement $D_s \rightarrow 0$, the strengthening slope dramatically increases to stop the same given rupture. At the limit $D_s = 0$, the strengthening slope has to be infinite in order to stop the rupture: this is the rigid case. In a sense, the strengthening barrier appears as a kind of regularization of the rigid barrier.

4.2. The case of a strengthening barrier with positive stress drop ($\eta > 0$)

We have shown that strengthening barriers are able to stop the rupture process, depending on the local crack growth resistance. In the following we study the influence of the initial size of the weak zone ($2a$)

on the ability of a given barrier to stop the rupture propagation. The friction parameters are the following: $D_s = 0.04\,\text{m}$, $D_c = 0.04\,\text{m}$, $S_s = 10\,\text{m}^{-1}$ and $S_w = 11\,\text{m}^{-1}$ for the barriers (derived from Fig. 6); $D_s = 0\,\text{m}$, $D_c = 0.04\,\text{m}$, $S_w = 1\,\text{m}^{-1}$ in the weak zone. With such parameters, the stress drop is the same all along the fault. That is the stress drop is positive in both the weak zone and the strengthening barriers,

$$g(x) = \begin{cases} S(\mu_s - S_w w(t_f, x, 0)/2)w(t_f, x, 0), & \text{for} & w(t_f, x, 0) < D_c \\ S(\mu_s - \mu_d)D_c/2 + S\mu_d w(t_f, x, 0), & \text{for} & w(t_f, x, 0) \geq D_c \end{cases} \tag{18}$$

as observed in friction experiments (Ohnaka and Yamashita, 1989).

Figs. 7–9 present the simulation of the rupture propagation on the fault in three different cases. The first case corresponds to a weak zone of length $2a = 2000\,\text{m}$. At time $t = 0\,\text{s}$, a small perturbation is applied at the center of the fault. This perturbation, which evolves into a dynamic instability that grows exponentially with time as the friction decreases from τ_s down to τ_d (initiation phase). As the stress reaches the dynamic friction at some patch on the weak zone, a crack front appears and propagates away on the fault until it reaches the strengthening barriers. Fig. 7 shows that in the case of a weak zone of length $2a = 2000\,\text{m}$, the barriers resist to the rupture and completely stop the propagation. Reflected waves heal the rupture inside the weak zone. The crack front is not able to propagate inside the barriers, but it turns out to a pulse of small and decaying amplitude that is actually associated with the crack-arrest zone described in Section 3.3. The second case corresponds to a weak zone of length $2a = 3000\,\text{m}$. Fig. 8 looks like Fig. 7 and exhibits the same main characteristics. However, in this case the barriers begin to fail as the reflected healing waves reach them. This progressive failure propagates at a very slow speed and stops over a distance of less than 200 m. This case appears like the limit case. This is confirmed by Fig. 9 that corresponds to the case of a weak zone of length $2a = 4000\,\text{m}$. In this case, the barriers are not able to stop the rupture. However, the propagation of the rupture front through the barriers is slightly delayed, and the rupture velocity is really slow but accelerating. This delay before the rupture of the barrier has been observed in the kinematic model of the rupture of the Landers earthquake. Campillo and Archuleta (1994) have observed that the rupture

propagation is stopped for a moment of a few seconds before it breaks a resisting zone. Figs. 7–9 demonstrate that the strengthening barriers are able to stop the rupture propagation in the case of small rupture patches. That is to say that unlike rigid barriers, strengthening barriers are able to store only a finite quantity of energy. The density of energy released in the weak zone is given by

Since $w_f(t, x, 0)$ scales with the weak zone length $2a$, the energy released in the weak zone, defined by

$$G = \int_{-a}^{a} g(x)\,\mathrm{d}x \tag{19}$$

scales with a^2, for large weak zone length, the strengthening barrier cannot counterbalance the rupture energy and the barrier fails. Since the barrier failure is associated with a positive stress drop, the rupture front propagation through the barrier is possible, as commonly observed at the scale of the laboratory friction experiments.

4.3. The case of a strengthening barrier with no stress drop ($\eta = 0$)

We aim to show in this section that the rupture propagation can also be stopped independently from the size of the rupturing patch by strengthening barriers with no stress drop (or negative stress drop). The local friction law parameters in the strengthening barriers are the following: $D_c = 0.04\,\text{m}$, $D_s = 4 \times 10^{-4}\,\text{m}$, $S_s = 100\,\text{m}^{-1}$, $S_w = 1\,\text{m}^{-1}$. Fig. 10 shows the complete rupture process computed with these parameters. The rupture develops on the weak zone and propagates through the barriers with a decreasing dislocation speed. Since $\mu_d = \mu_s$ in the barriers, they fail without any positive stress drop, i.e. without releasing energy. Therefore, the rupture will stop independently from the weak zone size. It is worth noting that the rupture may propagate over a great distance without any positive stress drop. As stated by Bonafede et al. (1985) in the quasistatic case, the distance of rupture propagation inside the barrier depends on the relative magnitude of the stress drop inside the weak zone and inside the barrier.
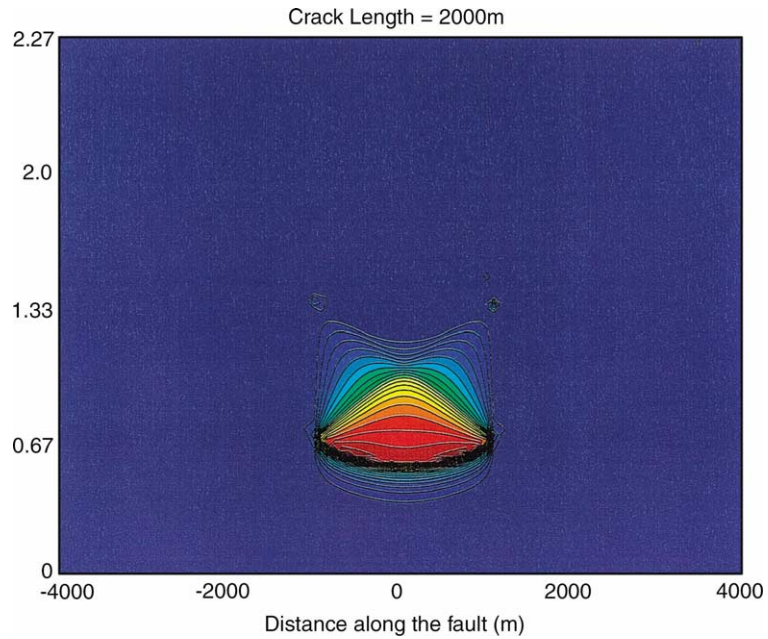
Fig. 7. Slip velocity evolution all along the fault for a weak zone size of $2a = 2000$ m. At $t = 0$ s, a small perturbation is applied at $x = 0$ m. This perturbation gives birth to a dynamic instability with an exponential time growth. At time $t \approx 0.6$ s, the crack front appears and propagates on the fault with an apparent supersonic velocity. At $t \approx 0.67$ s the crack front reaches the strengthening barriers and stops almost instantaneously. Reflected waves heal the rupture inside the weak zone. Computation achieved for a grid step $\Delta x = 10$ m.
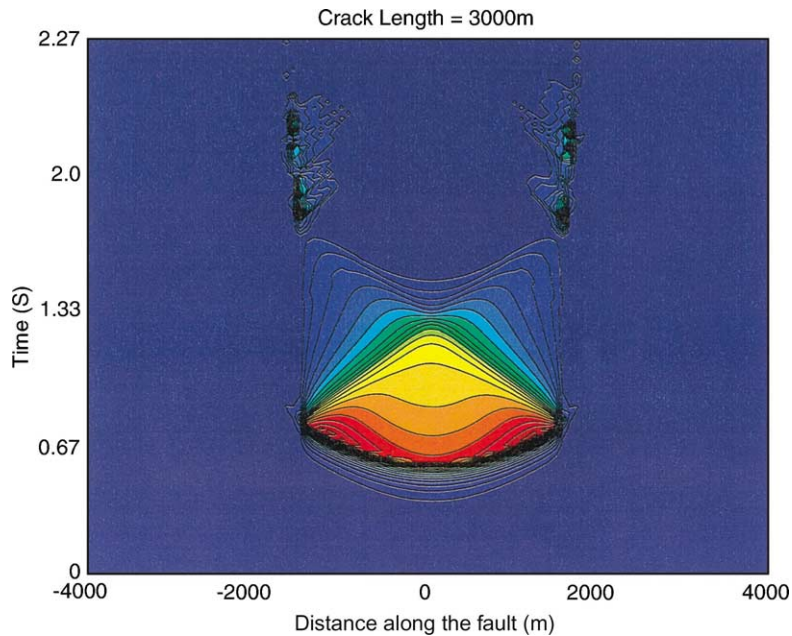

Fig. 8. Slip velocity evolution all along the fault for a weak zone size of $2a = 3000$ m. The figure exhibits the same characteristics as Fig. 7, except that in this particular case the barriers begin to fail as the reflected waves reach them (at $t \approx 1.6$ s). This progressive failure propagates at a very slow speed and rapidly stops (at $t \approx 2.1$ s). The dislocation speed is about 1 m s^{-1} inside the barrier. The maximum of the dislocation speed in the weak zone is about 0.6 m s^{-1}. Computation achieved for a grid step $\Delta x = 10$ m.
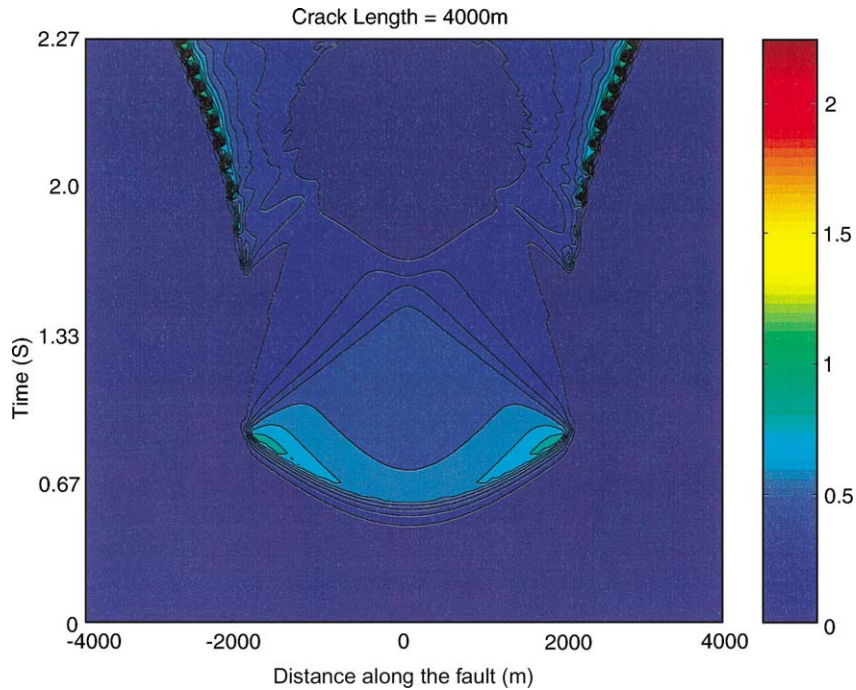
Fig. 9. Slip velocity evolution all along the fault for a weak zone size of $2a = 4000$ m. The barriers stop the rupture for a while but fail progressively. The rupture propagates inside the barrier at a slow but accelerating speed. The dislocation speed inside the weak zone is about $0.8 \, \mathrm{m\,s^{-1}}$, and about $2 \, \mathrm{m\,s^{-1}}$ inside the barriers. Computation achieved for a grid step $\Delta x = 10$ m.
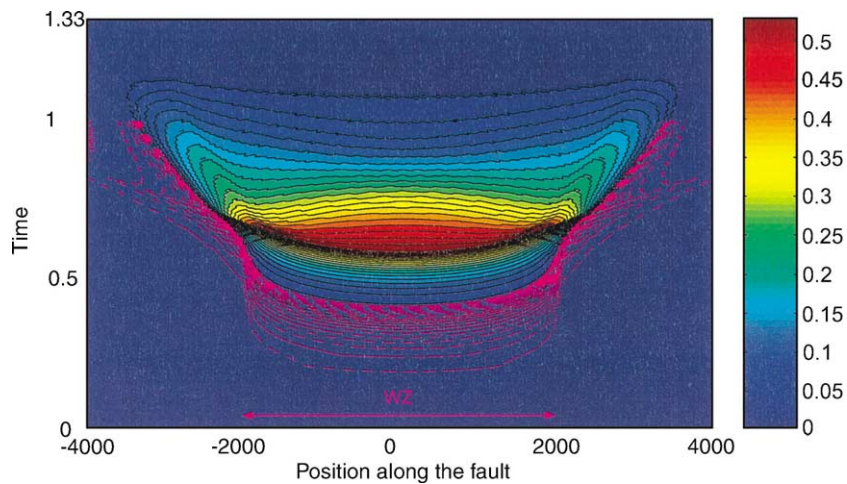

Fig. 10. Time evolution of the slip velocity on a weak zone surrounded by zero stress drop strengthening barriers. The rupture develops on the weak zone and reach the barriers. Then, the barriers fail over a distance of half the weak zone length. The rupture velocity inside the barrier is lower than the S-wave velocity. $D_c = 0.04$ m, $D_s = 4e - 4m$, $S_s = 100$, $S_w = 1$. With these parameters, the rupture propagates inside the barriers without any stress drop until the energy released in the weak zone is frittered away. Computation achieved for a grid step $\Delta x = 10$ m.

4.4. Analogy with the static homogeneous analysis

Chen and Knopoff (1986) have analyzed the static (residual) stress distribution along an infinite fault under a homogeneous linear slip-weakening friction law. They proved that it exists a peculiar distribution without any singularity. They found that for all $\gamma < \gamma_0 = 0.6219$ where γ is given by

$$\gamma = \frac{\tau_y^\infty - \tau_d}{\tau_s - \tau_d} \tag{20}$$

there exists a critical length of the slipping zone characterized by $a_c = a_c(\gamma, \alpha)$ and $b_c = b_c(\gamma, \alpha)$. Indeed the slip displacement along the fault has the following distribution:

$$\begin{aligned}
w(x, 0) &\geq D_c, && \text{for} \quad |x| \leq a_c \\
0 &< w(x, 0) < D_c, && \text{for} \quad a_c < |x| < b_c \\
w(x, 0) &= 0, && \text{for} \quad |x| \geq b_c
\end{aligned} \tag{21}$$

If $\gamma \geq \gamma_0$ there is no equilibrium state associated without stress singularity. These conditions can be interpreted dynamically as critical conditions for further expansion of an initial fault. Actually if a slip event occurs on a finite patch of length less than $2a_c$ then the crack will reach the critical configuration described above. If the initial slipping patch has a length greater than $2b_c$ then the crack will never stop. This is always the case for $\gamma > \gamma_0 = 0.6219$. Let us draw now an analogy between the above homogeneous static analysis and the nonhomogeneous dynamic model considered in this paper. It turns out from the friction experiments that the strengthening slip D_s is small compared to the critical slip D_c, of the order of one-tenth or less. Consequently, we can neglect the strengthening part in order to compare our dynamic results with the static analysis of Chen and Knopoff (1986). We use the parameter η introduced in Section 2 to be analogous to γ. Figs. 7–9 present the computations for different weak zone size bounded by the same barriers, with the same η. We have the same value for η but different behaviors depending on the length of the weak zone, in agreement with Chen and Knopoff (1986). Indeed if the weak zone size is smaller than $2a_c(\eta)$ then the rupture will be stopped by the barriers. On the contrary, if the weak zone size is greater than $2a_c(\eta)$ then the rupture will propagate throughout the barriers because there is no admissible static configuration. Concerning Fig. 10, we have $\eta = 0$ ($\gamma = 0$).

In such a case, the critical patch length is $2a_c = +\infty$. Therefore, any rupture of any length will be arrested.

5. The self-healing slip pulse

A particular feature of the strengthening behavior is shown by the dashed lines in Fig. 10. These lines describe the small amplitude evolution of the slip velocity in a range of 0–0.01 m s^{-1}. In the weak zone, these lines are in conformity with the large amplitude evolution of the slip velocity: they describe the initiation phase. Inside the barriers, these lines are no more in conformity with the large amplitude evolution (that is rapidly stopped). They show the small and decaying amplitude of the self-healing slip pulse. As expected, the distance of propagation of the pulse decreases with the strength of the barrier. This slip resisting pulse is associated with the crack-arrest zone and is in fact responsible for the small amount of slip observed in it. Fig. 11 represents the slip velocity evolution along the half fault surface. To emphasize on the self-healing slip pulse, we have considered in this simulation a weak zone of length $2a = 2000$ m limited by a strengthening barrier of growing resistance. The rupture front is clearly visible on Fig. 11 and obviously deviates as it enters the resisting zone, which signifies that the rupture front velocity is rapidly decreasing. The interesting feature of Fig. 11 is the self-healing pulse that is observed in the direction of the crack propagation. Both the pulse width and amplitude are rapidly vanishing as it propagates inside the barrier. This allows to distinguish the pulse from a propagating wave. The pulse is associated with the crack-arrest zone already described, and corresponds to the beginning of slippage inside the barrier. Since the law is locally a strengthening law, this slippage is rapidly stopped. It is worth noting that Perrin et al. (1995), using a rate and state friction law and variable state of stress along the fault surface, have shown the possibility for the rupture to propagate as a crack or as a self-healing slip pulse. The crack-arrest zone and the corresponding self-healing slip pulse are directly related to the strengthening behavior. Consequently, both their size and amount of slip are linked to the strengthening parameters of the barrier. It is therefore possible to produce a wide variety of slip distribution, depending on the friction parameters along the fault surface.
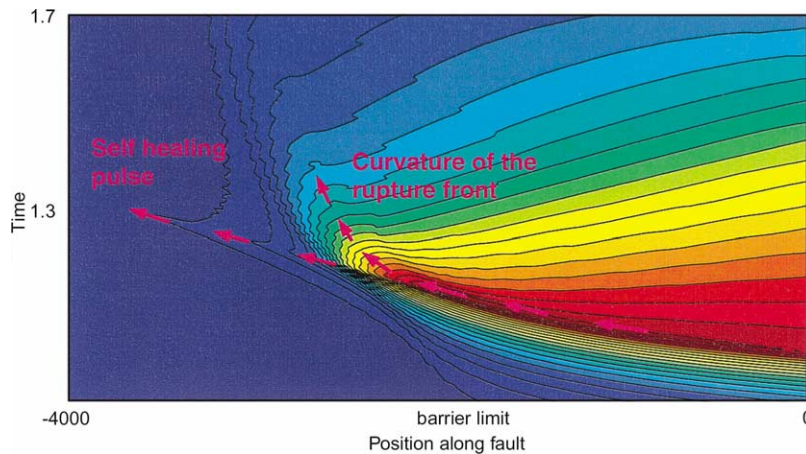
Fig. 11. Relation between the crack-arrest zone and the self-healing slip pulse. The rupture nucleates and propagates in the weak zone. As the rupture enters the increasing strength barrier, the crack front obviously deviates, which signifies a rapid decrease in the rupture velocity. The self-healing pulse appears in the continuity of the crack front. Computation achieved for a grid step $\Delta x = 10\,\text{m}$.

6. Strengthening barriers and fault growth

The strengthening barrier model provides a possible mechanism for the extension of fault length throughout the repetition of earthquakes or tectonic loading. Geological observations permit to reconstruct the evolution of discontinuities, i.e barriers, along the normal fault systems of the Afar region (Manighetti et al., 2001). Among many other results, it was found that the fault length was increasing at a mean rate of 15 cm per year. The strengthening barrier model is able to reproduce this feature. In this model, each rupture event is stopped over two crack-arrest zones associated with small amount of slip and stress concentration. These zones, in which the slip is less than the strengthening slip D_s correspond to zones of damaging of the barriers. The reoccurrence of earthquakes on the same fault implies a step by step increase in the slip, that is, after each event the damaging of the barrier increases. At some time, the slip eventually becomes greater than D_s at the transition from the weak zone to the strengthening barrier. The transition zone then describes the weakening part of the friction law: the next event on the fault will break this transition zone, extending the fault length. Since the strengthening model includes an explicit reference to the stress level, it makes it possible to consider also the effect of tectonic loading both on rupture behavior

and on fault length increase. As a point of fact, a given strengthening barrier may eventually resist and stop a given rupture process. If the same barrier is progressively loaded by tectonics, it will probably be broken by the same rupture event. One must observe that the tectonic loading will progressively increase the slip in the strengthening zones, contributing to a possible fault length extension during the seismic cycle. The strengthening barrier model therefore, accounts for the possible interaction between the regional stress field and the dynamic stress field emitted during the rupture propagation.

7. Conclusion

The strengthening barrier model provides response to several problems that arise when using a rigid barrier model. The use of smooth strengthening barriers removes the nonphysical shear stress singularity that is associated with the use of a rigid barrier. The slip distribution spreads *inside* the strengthening barrier over a crack-arrest zone. This zone corresponds to a damaging of the strengthening barrier, and is associated with small amount of slip. Depending on the strengthening parameters in the barrier, two arrest mechanisms are possible. The first one is associated with a null or negative stress drop in the barrier. This mechanism

is already well-known and is crack-size independent: the rupture stops because of a lack of energy. The second arrest mechanism is associated with a positive stress drop even inside the barrier. This mechanism is crack-size dependent. The resistance of a strengthening barrier is finite and depends on both the peak stress $\tau_p = S_s D_s$ and the strengthening slip D_s. Both mechanisms are associated with the crack-arrest zone and a self-healing slip pulse that hardly propagates inside the barrier and vanishes rapidly. Width and amplitude of this pulse are both controlled by the strengthening parameters, allowing a wide variety of slip distributions. Strengthening barriers are also consistent with recent strong motion inversions that shows the existence of patches associated with small amount of slip and increase in stress. The strengthening barrier model provides a possible model for fault length increase with time through the existence of a crack-arrest zone. The repetition of rupture events on the same fault progressively increases the damaging of the barriers that eventually fail, thus leading to a progressive increase in the fault length during the seismic cycle.

Acknowledgements

References

Ampuero, J., Vilotte, J., Sánchez-Sesma, F., 2001. Nucleation of rupture under slip dependent friction law: simple models of fault zone. J. Geophys. Res.

Barenblatt, G., 1959. The formation of equilibrium cracks during brittle fracture general ideas and hypotheses. J. Appl. Math. Mech. 23, 622–636.

Beroza, G., Mikumo, T., 1996. Short slip duration in dynamic rupture in the presence of heterogeneous fault properties. J. Geophys. Res. 101, 22449–22460.

Bonafede, M., Dragoni, M., Boschi, E., 1985. Quasi-static crack models and the frictional stress threshold criterion for slip arrest. Geophys. J. Roy. Astron. Soc. 83, 615–637.

Bouchon, M., Campillo, M., Cotton, F., 1998. Stress field associated with the rupture of the 1992 Landers, california, earthquake and its implications concerning the fault strength at the onset of the earthquake. J. Geophys. Res. 103, 21091–21097.

Burridge, R., 1973. Admissible speeds for plane-strain self-similar shear cracks with friction but lacking cohesion. Geophys. J. Roy. Astron. Soc. 35, 439–455.

Campillo, M., Archuleta, R., 1994. A rupture model for the 28 June 1992, Landers, California, earthquake. Geophys. Res. Lett. 20, 647–650.

Campillo, M., Ionescu, I., 1997. Initiation of antiplane shear instability under slip dependent friction. J. Geophys. Res. 102, 20,363–20,371.

Chen, Y., Knopoff, L., 1986. Static shear crack with a zone of slip-weakening. Geophys. J. Roy Astron. Soc. 87, 1005–1024.

Das, S., Aki, K., 1977. Fault plane with barriers: a versatile earthquake model. J. Geophys. Res. 82, 5658–5670.

Dascalu, C., Ionescu, I., Campillo, M., 2000. Fault finiteness and initiation of dynamic shear instability. Earth Plan. Sci. Lett. 177, 163–176.

Day, S., 1982. Three-dimensional simulation of spontaneous rupture: The effect of nonuniform prestress. Bull. Seismol. Soc. Am. 72, 1881–1902.

Husseini, M., Jovanovitch, D., Randall, M., Freund, L., 1975. The fracture energy of earthquakes. Geophys. J. Roy. Astron. Soc. 43, 367–385.

Ida, Y., 1972. Cohesive force along the tip of a longitudinal shear crack and Griffith's specific surface energy. J. Geophys. Res. 77, 3796–3805.

Ionescu, I., Campillo, M., 1999. Influence of the shape of friction law and fault finiteness on the duration of initiation. J. Geophys. Res. 104, 3013–3024.

Kame, N., Yamashita, T., 1999. A newlight on arresting mechanism of dynamic earthquake faulting. Geophys. Res. Lett. 26, 1997–2000.

Knopoff, L., Landoni, J., Abinante, M., 2000. Causality constraint for fractures with linear slip-weakening. J. Geophys. Res. 105, 28035–28043.

Madariaga, R., 1976. Dynamics of an expanding circular fault. Bull. Seism. Soc. Am. 66, 639–666.

Madariaga, R., Olsen, K., Archuleta, R., 1998. Modeling dynamic rupture in a 3D earthquake fault model. Bull. Seism. Soc. Am. 88, 1182–1197.

Manighetti, I., King, G., Scholz, C., Gaudemer, Y., Doubre, C., 2001. Slip accumulation and lateral propagation of active normal faults in afar. J. Geophs. Res. 106, 13667–13696.

Ohnaka, M., 1992. Earthquake source nucleation: a physical model for short-term precursors. Tectonophysics 211, 149–172.

Ohnaka, M., 1996. Nonuniformity of the constitutive law parameters for shear rupture and quasistatic nucleation to dynamic rupture: a physical model of earthquake generation processes. Proc. Natl. Acad. Sci. U.S.A. 93, 3795–3802.

Ohnaka, M., Yamashita, T., 1989. A cohesive zone model for dynamic shear faulting based on experimentally inferred constitutive relation and strong motion source parameters. J. Geophys. Res. 94, 4089–4104.

Ohnaka, M., Akatsu, M., Mochuzuki, H., Odedra, A., Tagashira, F., Yamamoto, Y., 1997. A constitutive law for the shear failure of rock under lithospheric conditions. Tectonophysics 277, 1–27.

Olsen, K., Madariaga, R., Archuleta, R., 1997. Three-dimensional dynamic simulation of the 1992 Landers earthquake. Science 278, 824–838.

Perrin, G., Rice, J., Zheng, G., 1995. Self healing slip pulse on a frictional surface. J. Mech. Phys. Solids 43, 1461–1495.

Rice, J., Simmons, D., 1976. The stabilization of spreading shear faults by coupled deformation-diffusion effects in fluid-injected porous media. J. Geophys. Res. 81, 5322–5334.

Streiff, D., Bouchon, M., 1997. Propagation of a shear crack on a nonplanar fault: a method of calculation. Bull. Seism. Soc. Am. 87, 61–66.

Voisin, C., Ionescu, I., Campillo, M., Hassani, R., Nguyen, Q., 2002. Process and signature of initiation on a finite fault system: a spectral approach. Geophys. J. Int. 148, 120–131.